A structural study and some magnetic properties of YCo12-xFexB6 (x = 0 to 4.5) solid solution

B. Vallet-Simond, S. Giron, L. V. B. Diop, Olivier Isnard

A structural study and some magnetic properties of $YCo_{12-x}Fe_xB_6$ (x = 0 to 4.5) solid solution

B. Vallet-Simond[1], S. Giron[2], L. V. B. Diop[3], O. Isnard[1]

[1]*Université Grenoble Alpes, Institut Néel, CNRS, BP166X, 38042 Grenoble Cédex 9, France*

[2]*Institute of Materials Science, Technical University of Darmstadt, D-64287 Darmstadt, Germany*

[3]*Université de Lorraine, CNRS, IJL, F-54000 Nancy, France*

Abstract

We report on the effects of Fe substitution on the structural and magnetic properties of the $YCo_{12-x}Fe_xB_6$ series of compounds by combining scanning electron microscopy, energy dispersive X-ray microanalysis, X-ray powder diffraction and magnetic measurements. The rhombohedral $R\bar{3}m$ structure of the $YCo_{12-x}Fe_xB_6$ is retained up to about x= 4.5 Fe atom per formula unit, a value that we assign to the estimated solubility limit for polycrystalline samples. The unit cell is found to expand regularly upon increasing the iron content with a rate of 1.55 $Å^3$ per Fe atom, the expansion being larger along the basal plane. Clues for the preferential substitution scheme of Fe for Co are discussed. It is also shown that Fe for Co substitution induces dramatic changes on the magnetic properties such as a strong decrease of the ordering temperature and a significant reduction of the spontaneous magnetization.

Keywords: rare-earth – transition metal intermetallics, scanning electron microscopy, X-ray diffraction, crystal structure, phase diagrams, magnetic measurements.

1. Introduction

Intermetallic compounds of rare-earth R and transition metals T are widely studied for their enhanced magnetic properties leading to numerous magnetic applications such as high performance permanent magnets, magnetostrictive effects used in sensors and actuators, magnetocaloric effects for magnetic cooling. The improvement of the understanding of the structural properties and or physical properties of such intermetallic compounds is consequently of outmost interest to master the applications of these materials, discover and design new ones with optimized properties. Here we focus our attention on a rare-earth intermetallic compound of $RT_{12}B_6$ type, which have been reported originally by Niihara and Yajima [1], followed by Kuz'ma *et al.* [2] and later studied by other research teams [3,4]. This family of compounds crystallizes in the rhombohedral $SrNi_{12}B_6$-type structure (space group $R\bar{3}m$). In such a crystal lattice, the T atoms are located in two inequivalent crystallographic positions (18*g* and 18*h*) with the R and B atoms occupying the 3*a* and 18*h* Wyckoff sites, respectively. The $RCo_{12}B_6$ intermetallics are stable along the whole rare-earth series with unit-cell parameters that follow the conventional lanthanide contraction. By contrast, $LaFe_{12}B_6$ is the only stable Fe-based member of the $RT_{12}B_6$ ternary system. Although being the first Fe-based alloy of the $RT_{12}B_6$ family to be discovered, $NdFe_{12}B_6$ is metastable [5]. Figure 1 depicts the local atomic environment of Y and the two Co sites. The Y atom (3*a* Wyckoff site) is surrounded by 24 near neighbours, half of which are Co-18*g* in addition to 6 Co-18*h* and 6 B atoms. The local environment of Co-18*g* position is made of 13 atoms, 2 of which are Y ones, 4 Co-18*h* type, 4 B neighbours and 3 are Co-18*g* ones. The Co-18*h* site is also surrounded by 13 near neighbours, however, here one finds only one Y atom, 5 Co located at 18*h*, 3 B atoms and 4 Co-18*g* neighbours. Remarkably short Co-B interatomic distances have been reported in $YCo_{12}B_6$ ($<d_{Co-B}> = 2.05$ Å) [6].

Interestingly, intriguing magnetic properties were recently reported in $LaFe_{12}B_6$ compound [7] shedding light on the itinerant electron magnetism of iron. Indeed $LaFe_{12}B_6$ phase exhibits huge metamagnetic transition and large magnetocaloric effect [8]. This has triggered a regain of interest for the investigation of the fundamental physical properties of $RT_{12}B_6$ compounds [9]. The interest for the $YCo_{12-x}Fe_xB_6$ series of compounds stems from the unusual behaviour of the itinerant electron metamagnet $LaFe_{12}B_6$ [7, 10, 11]. The present study is devoted to the investigation of the Fe solubility in $YCo_{12}B_6$ compound and the effects of Fe for Co substitution on the structural and magnetic properties. $YCo_{12}B_6$ has been reported to be a ferromagnetic (FM) compound with a remarkably low Curie temperature (T_C = 152 K) despite

the high Co content. Co-based $RT_{12}B_6$ type compounds have attracted much interest and have been extensively investigated over the last decades [9, 12-14] ($RCo_{12}B_6$ with R=Y, Ce, Nd, Gd, Ho).

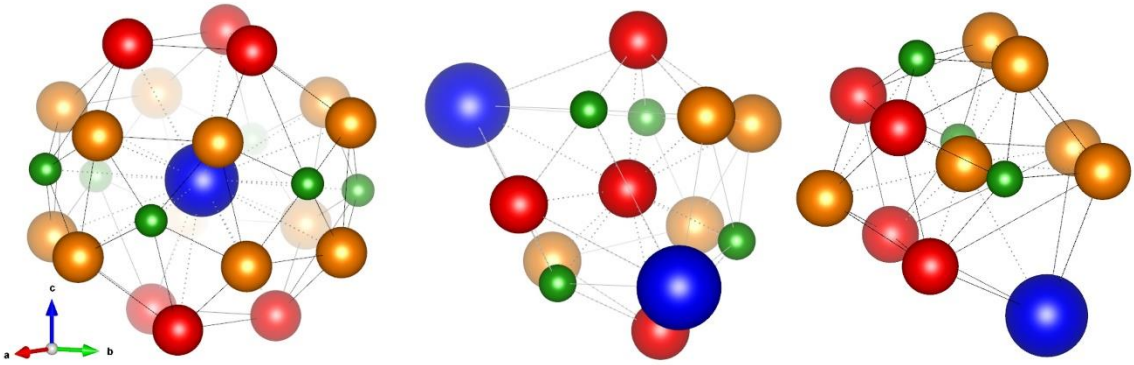

Figure 1: Schematic drawing of the 3*a*, 18*g*, 18*h* atomic positions from left to right respectively. The 18*g*-Co/Fe atoms are plotted in red. The 18*h*-Co/Fe atoms are represented by orange balls, the B atoms in small green ones and the rare earth elements in big blue balls.

2. Experimental techniques

$YCo_{12-x}Fe_xB_6$ samples with nominal compositions ranging from $x = 0$ up to $x = 8$ (x = 0; 0.5; 1; 1.5; 2; 2.5; 3; 3.5; 4; 4.5; 5; 5.5; 6; 7; 8) have been prepared and characterized by systematic investigation using X-ray diffraction and electron scanning microscopy technique. The $YCo_{12-x}Fe_xB_6$ alloys were synthetized by arc melting the mixture of high-purity elements (Y: 99.9 wt. %, Co: 99.95 wt. %, Fe: 99.9999 wt. % and B 99.5 %.) under a purified argon gas atmosphere. To ensure homogeneity, each alloy (total weight ranging typically between 3 and 3.5 g) was melted five times with the button being flipped over after each re-melting. The weight losses after arc-melting were low (< 0.5 wt.%). The obtained ingots were wrapped in tantalum foil and then sealed in evacuated silica tubes and subsequently placed at 900° C in a resistive furnace for three weeks. The annealed samples were characterized at room temperature by standard X-ray powder diffraction using a Bruker D8 Endeavour diffractometer (Cu Kα radiation) in reflection mode with the Bragg–Brentano geometry over an angular 2θ range from 10° to 100° and a scan step of 0.01°. Rietveld refinements of the diffraction patterns were performed using the FullProf suite software package [15]. Structural parameters and phase quantities were determined. The X-ray fluorescence radiation has been

removed from the diffraction pattern by precise selection in energy of the semiconductor detector signal.

Scanning electron microscopy (SEM) images were collected using back scattered electrons (BSE) in a Tescan VEGA3 SBH ($0 < x \leq 4$) and a Zeiss Ultra+ ($x \geq 4.5$). Composition analysis was carried out via energy dispersive X-ray spectroscopy (EDX) in the Tescan microscope with an EDAX Octane Plus detector and with a QUANTAX EDS from BRUKER in the Zeiss microscope. SEM coupled with EDX analysis have been used systematically to perform metallography investigation on polished surface of each ingot in order to identify the phases and their composition. The composition has been determined on the basis of *L* emission of yttrium and *K* emission of Co and Fe. ZAF type corrections have been applied to the EDX quantification results.

Magnetic measurements were undertaken on powder samples in static magnetic fields of up to 9 T at temperatures between 2 and 300 K using a vibrating-sample magnetometer (Quantum Design PPMS-9). All the magnetization data in the present study were corrected for the presence of the minor ferromagnetic impurity phase to get the intrinsic magnetic properties of the $YCo_{12-x}Fe_xB_6$ compounds.

3. Results and discussion

The phase composition study performed by scanning electron microscopy reveals the presence of a main phase up to about $x = 4.5$. This main phase is featured by an yttrium versus transition metal atomic ratio corresponding to the $Y(Co,Fe)_{12}B_6$ expected 1/12 concentration. The boron atom is too light to be accurately detected by this experimental technique. This study also shows for all samples the presence of traces of a minority phase which does not contain yttrium and appears in dark grey in the BSE images of Figure 2 as well as another impurity trace that is richer in rare earth. According to microanalysis, the Co/Fe ratio varies along the $YCo_{12-x}Fe_xB_6$ series. For samples with nominal composition $x \geq 5$, a large amount of impurity phases are observed as can be seen from Figure 2f. For such type of samples, several phases are coexisting in the ingot including an yttrium rich one appearing as white on the BSE images. The matrix phase (intermediary grey) corresponds to the $Y(Co,Fe)_{12}B_6$ compounds up to $x = 4$ as can be seen on figure 2a to 2e. At $x = 5.5$, the sample is multiphase where we can distinguish best all the impurities encountered in those samples. In white, we have the phases richest in heavy elements [Y_2O_3 or $Y(Co,Fe)_4B_4$], in black/dark grey we have the light phases, i.e., $(Co,Fe)_2B$ or α-(Co,Fe). In intermediary grey, we find again the $Y(Co,Fe)_{12}B_6$ phase. Note that

all EDX measurements on this phase occurred on phase islet big enough for the interaction pears, not shown on figure 2f.

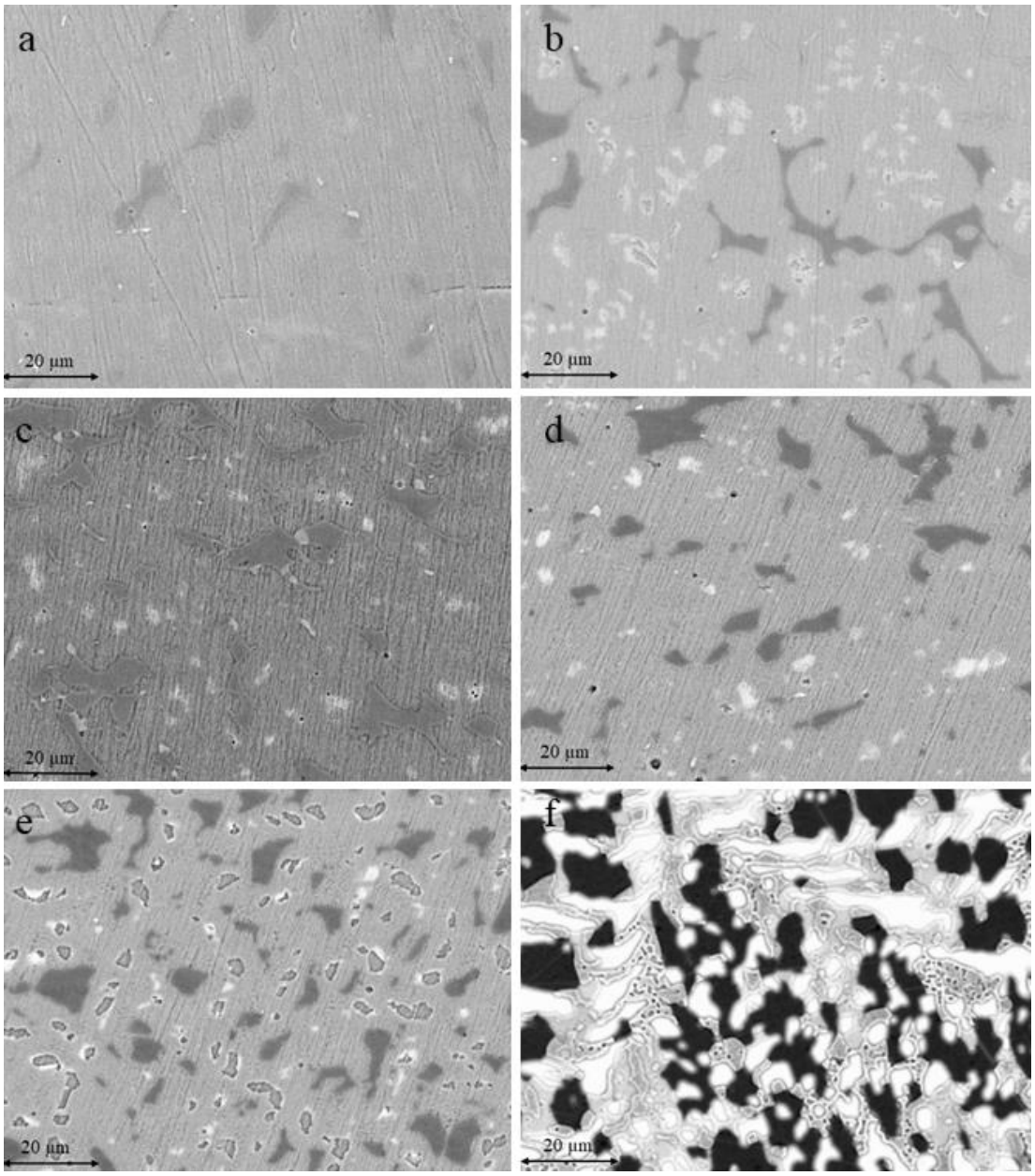

Figure 2: Scanning electron image obtained from backscattering electron detection mode on $YCo_{12-x}Fe_xB_6$ series of compounds figure a, b, c, d, e and f correspond to composition x = 0, 1, 2, 3, 4 and 5.5 respectively. Note that sample for x = 5.5 has been measured using a different scanning electron microscope and energy dispersive X-ray analysis setup (Zeiss Ultra+ with the Bruker EDS system). From a to c: White phase: Y_2O_3 / Intermediary grey: $Y(Co,Fe)_{12}B_6$ / Dark grey: (Co,Fe)-B. From d to f: White phase: Y_2O_3 / Intermediary grey "light": $Y(Co,Fe)_4B_4$ / Intermediary grey "dark": $Y(Co,Fe)_{12}B_6$ / Dark grey: (Co,Fe) + $(Co,Fe)_2B$.

Nominal *x*	Measured Fe/Co ratio	Ideal Fe/Co ratio	Measured Y/(Co,Fe) ratio	Ideal Y/(Co,Fe) ratio
0	0	0	0.069(12)	
1	0.081(9)	0.091	0.071(12)	
2	0.175(18)	0.200	0.070(12)	0.083
3	0.297(27)	0.333	0.070(12)	
4	0.407(36)	0.500	0.074(12)	
5.5	0.515(40)	0.846	0.077(12)	

Table 1: Energy dispersive X-ray spectroscopy quantitative results of the $YCo_{12-x}Fe_xB_6$ phases identified using the electron beam microscopy. The boron quantity was not accessible through this method.

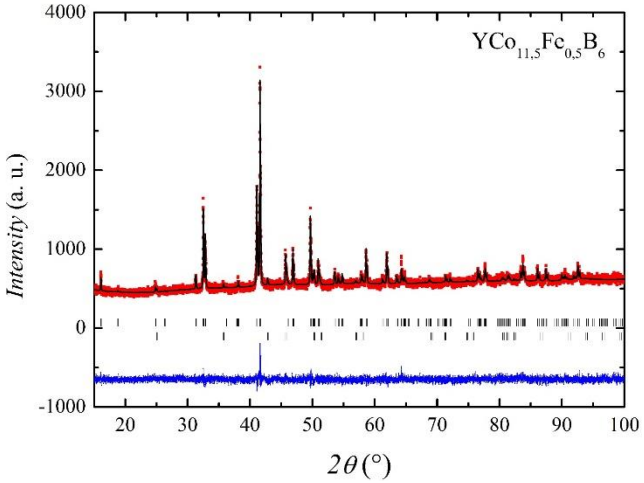

Figure 3: Rietveld refinement of the X-ray diffraction pattern recorded at room temperature for $YCo_{11.5}Fe_{0.5}B_6$. The first refined phase is $YCo_{11.5}Fe_{0.5}B_6$ (R_B = 14.6(%)) and the second one is the impurity $(Co,Fe)_2B$ (R_B = 28.5(%)). The agreement factors were R_{exp} = 4.15(%), R_{wp}=*4.57* (%).

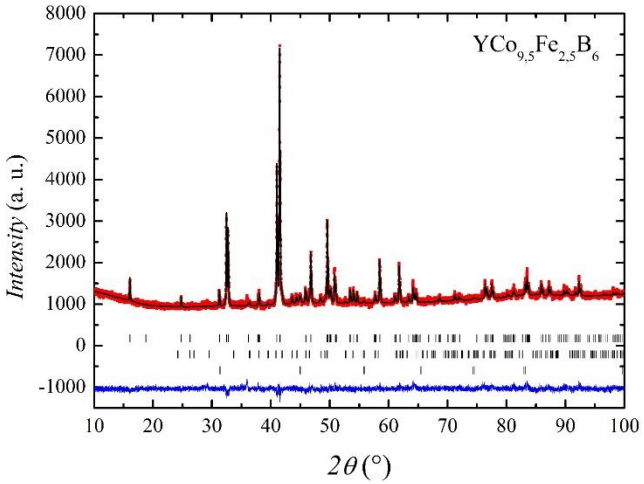

Figure 4: Rietveld refinement of the X-ray diffraction pattern recorded at room temperature for $YCo_{9.5}Fe_{2.5}B_6$. The first refined phase is $YCo_{9.5}Fe_{2.5}B_6$ (R_B = 14.2(%)), the second one is the impurity $(Co,Fe)_3B$ (R_B = 34.0(%)) and the third one is (Co,Fe) (R_B = 17.6(%)). The agreement factors were R_{exp} =2.93(%), R_{wp}=*3.59*(%).

$YCo_{12-x}Fe_xB_6$	a (Å)	c (Å)	V (Å^3)	T_C (K)
0	9.437 (6)	7.436 (5)	573.5 (6)	155 (3)
0.5	9.442 (6)	7.438 (5)	574.2 (6)	151 (3)
1	9.448 (6)	7.439 (5)	575.1 (6)	139 (3)
1.5	9.453 (6)	7.442 (5)	575.9 (6)	124 (3)
2	9.459 (6)	7.445 (5)	576.9 (6)	107 (3)
2.5	9.462 (6)	7.448 (5)	577.5 (6)	92 (3)
3	9.467 (6)	7.451 (5)	578.4 (6)	73 (3)
3.5	9.471 (6)	7.453 (5)	579.1 (6)	60 (5)
4	9.475 (6)	7.456 (5)	579.7 (6)	54 (5)
4.5	9.474 (6)	7.460 (5)	579.9 (6)	
5	9.474 (6)	7.460 (5)	580.1 (6)	

Table 2: Unit cell parameters of the $R\bar{3}m$ rhombohedral crystal structure and Curie temperature of the $YCo_{12-x}Fe_xB_6$ compounds

A Rietveld refinement of the diffraction pattern for the sample with nominal composition $x = 0.5$ is presented in Figure 3. The analysis of the diagram reveals that the main phase, identified as $YCo_{11.5}Fe_{0.5}B_6$, corresponds to about 91(3) wt. % of the sample confirming the above discussed results from electron microscopy. The obtained lattice parameters are a = 9.437 Å and c = 7.436 Å. The minority phase can be indexed on the basis of the tetragonal $I4/mcm$ space group and correspond to the Co_2B type phase. Its content amounts to 9(3) wt.% for the $YCo_{11.5}Fe_{0.5}B_6$ sample. Rietveld analysis of the $x = 2.5$ X-ray diffraction pattern – figure 4 – confirms the presence of the $R\bar{3}m$ structure as the majority phase with $(Co,Fe)_3B$ ($Pnma$) as impurity and traces of α−(Fe,Co). Similar behaviour was observed for the X-ray diffraction pattern corresponding to x = 0, 1, 2, 3, 4, and 4.5 (see figure 5). The $Y(Co,Fe)_{12}B_6$ phase is still present for $x = 5.5$ but as minority phase, and its amount significantly decreases for larger Fe content. It is noteworthy that for $x = 6$ and above, the $YT_{12}B_6$ type phase is not detected in the diffraction patterns. The only remaining phases are $(Co,Fe)_2B$, α−Fe, and $Y(Co,Fe)_4B_4$. Table 1 associated with figure 2 displays measurements done only on the 1:12:6 phase of interest. We see that until $x = 4$, the measured ratios of the different chemical species are in agreement with the values calculated for an ideal sample. Note that there seems to be an overall tendency to overestimate the Co content. For $x = 5.5$, we see that the Fe/Co ratio is much lower than what is expected and is more in accord with what could be measured for $x = 4$ or 4.5. We attribute this to the fact that the solubility limit is reached around this value of Fe content and it is in agreement with the results of the XRD patterns Rietveld analysis.

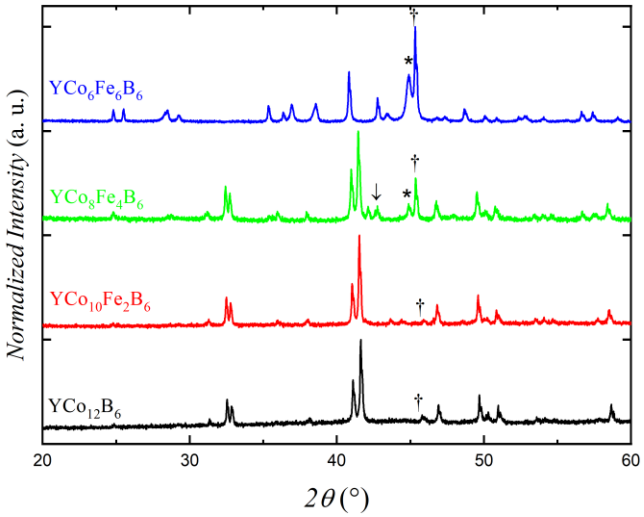

Figure 5: Selection of X-ray diffraction patterns recorded at room temperature for several nominal compositions of $YCo_{12-x}Fe_xB_6$. The main Bragg peaks belonging to impurity phases are indicated by symbols. The dagger marks the presence of $(Co,Fe)_2B$, the asterisk is for the α-(Fe,Co) phase and the arrow refers to the presence of $Y(Co,Fe)_4B_4$. The diffraction patterns have been shifted vertically for clarity.

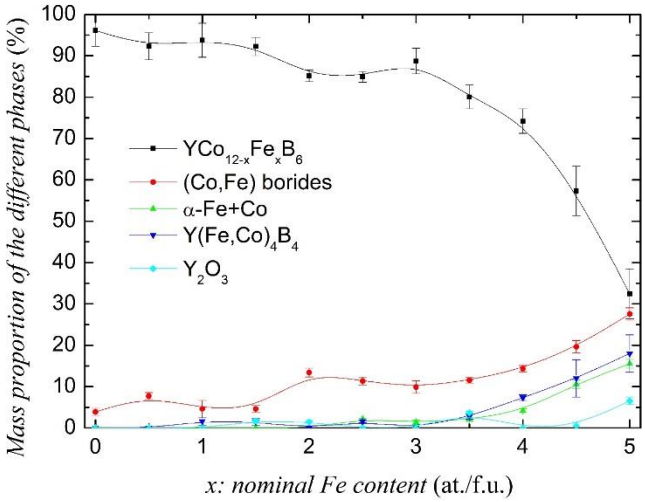

Figure 6: Mass fraction of the different phases versus nominal Fe content as derived from Rietveld refinements of the X-ray diffraction patterns for $YCo_{12-x}Fe_xB_6$ series.

The concentration of each phase has been determined from Rietveld analysis and the corresponding results are plotted in Figure 6. It clearly shows that up to x = 3 the samples contain a major phase $YCo_{12-x}Fe_xB_6$ with traces of transition metal borides $(Co,Fe)_2B$ (or $(Co,Fe)_3B$ for x = 2 and 2.5). For larger Fe content, the impurity concentration increases significantly, the main phase $YCo_{12-x}Fe_xB_6$ corresponding to 60% for x = 4.5. In addition, one can note the appearance of a large amount of $Y(Co,Fe)_4B_4$ and traces of Y_2O_3 impurities for x > 3.5. As can be seen from Figure 6, the $R\bar{3}m$ structure of the $YCo_{12-x}Fe_xB_6$ series is by far the major phase up to x = 4.5. Below this composition traces of $(Co,Fe)_2B$ phase are detected from X-ray diffraction. The mean transition metal boride phase content is estimated to about 9% up

to $x = 3$. Then it increases continuously. Above $x = 5$ the $(Co,Fe)_2B$ phase becomes predominant together with additional trace of alpha iron. Significant amount of $Y(Co,Fe)_4B_4$ phase [16] is noticeable for $x = 3.5$ and above. The phase identifications from X-ray diffraction have been confirmed by X-ray microanalysis using energy dispersive spectroscopy. Selected samples have been also studied by Electron microprobe analysis and wavelength dispersive spectroscopy in order to be more sensitive to the boron content. Combining these results with X-ray diffraction data discussed above, we conclude that the $YCo_{12-x}Fe_xB_6$ phase content start to decrease significantly when approaching the solubility limit of c.a. 4.5 Fe atom per formula unit and that it dramatically drops above.

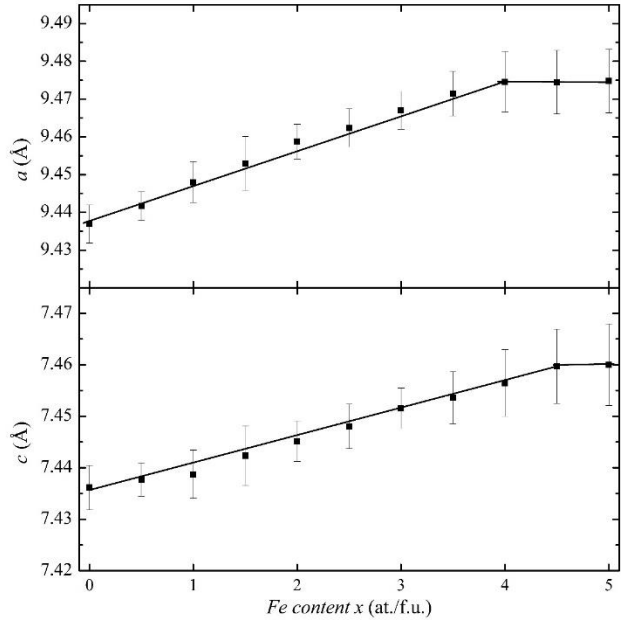

Figure 7: Lattice parameters, *a* and *c*, as a function of Fe content in $YCo_{12-x}Fe_xB_6$ series of compounds.

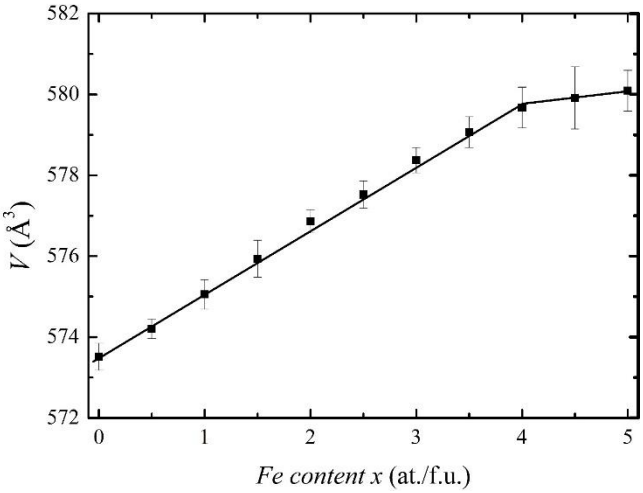

Figure 8: Unit-cell volume, *V*, as a function of Fe content in $YCo_{12-x}Fe_xB_6$ series of compounds.

The lattice parameters derived from Rietveld refinements of the X-ray diffraction patterns are plotted in Figures 7 and 8 and the corresponding values are summarized in Table 2 for all the studied compounds. Both lattice parameters, *a* and *c*, exhibit a linear behaviour and increase with the Fe content. The expansion rate amounts to $\Delta a/a$=0.399 % and $\Delta c/c$=0.273 % for *a* and *c* respectively thus leading to an overall volume expansion of $\Delta V/V$ = 1.07 %. It is interesting to notice that the *a* lattice parameter saturates at about 9.475 Å for $x \geq 4$. The *c* parameter also saturates but at a composition of x = 4.5 to a value of 7.460 Å. Combining these results with the ones discussed above we conclude that the solubility limit of Fe in the $YCo_{12-x}Fe_xB_6$ series of compounds is about x = 4.5. The unit cell expansion is more pronounced in the basal plane of the rhombohedral lattice. Overall, an expansion rate of 1.55 $Å^3$ per Fe atom is obtained along the $YCo_{12-x}Fe_xB_6$ series of compounds. The observed unit cell expansion reflects the largest atomic size of Fe whose metallic radius is 1.27 Å against 1.25 Å for Co according to the calculations of Teatum and Gschneidner [17]. The atomic positions derived from Rietveld refinements of the X-ray patterns of Figs. 3 and 5 are listed in table 3 for x = 0.5 and x = 2.5 respectively.

Wyckoff position	Fe content (at/f.u.)	*x/a*	*y/a*	*z/c*	Numbers of neighbours	Nature of neighbours
Y (3*a*)	Same for *x*=0.5 and 2.5	0	0	0	24	12 T_1, 6 T_2, 6 B
T_1 (18*g*)	*x*=0.5 *x*=2.5	0.3701(9) 0.3704(8)	0	0.5	13	3 T_1, 4 T_2, 4 B, 2 R
T_2 (18*h*)	*x*=0.5 *x*=2.5	0.4236(5) 0.4228(5)	0.5764(5) 0.5772(5)	0.0349(14) 0.0295(15)	13	4 T_1, 5 T_2, 3 B, 1 R
B (18*h*)	*x*=0.5 *x*=2.5	0.4928(40) 0.5043(53)	0.5072(40) 0.4957(53)	0.3126(92) 0.2667(99)	8	4 T_1, 3 T_2, 1 R

Table 3: Crystal structure parameters as derived from Rietveld refinement of the X-ray powder diffraction pattern for $YCo_{11.5}Fe_{0.5}B_6$ and $YCo_{9.5}Fe_{2.5}B_6$ compound.

The precise location of the Fe atoms within the crystal structure has not been determined here since Co and Fe have similar scattering length for X-ray diffraction due to

only one electron difference. The fact that the Fe atoms solubility limit is below $x = 6$, that is, below one half of the available transition metal positions, indicates that even in the hypothesis of a preferential location on one site, this site could not be fully occupied by Fe atoms in the Y containing compounds. Whereas for La the substitution is complete (complete solid solution); the end-member compounds $LaCo_{12}B_6$ and $LaFe_{12}B_6$ are stable. It is remarkable that for the Y containing phase it is already reduced by more than a factor 2.7. This is likely due to the smaller unit-cell volume of $YCo_{12}B_6$ compared to that of $LaCo_{12}B_6$. Indeed since Fe for Co substitution requires a significant lattice expansion, such substitution is expected to be more difficult in a constricted unit cell such as the Y one. ^{57}Fe Mössbauer spectroscopy and neutron diffraction studies on pseudo-ternary compounds of $R(Co,Fe)_{12}B_6$ [3,9,11] indicate that Fe shows a strong preferential occupation of the 18*h* site. Similar investigations would be interesting to perform on the present $YCo_{12-x}Fe_xB_6$ series of compounds to determine the precise substitution scheme of Fe within the rhombohedral crystal structure.

It is interesting to compare the Fe solubility limit obtained here for Y-based compound to that reported earlier for other isotype compounds such as La or Gd containing one. La being the largest among the lanthanides (metallic radius r_{La}=1.877Å [17]) and the Gd being located in the middle of the lanthanide series (r_{Gd}=1.801 Å close to that of yttrium r_Y=1.773 Å [17]). The Fe for Co substitution has been well studied in $LaCo_{12}B_6$ [3]. Whereas a complete solid solution exists between $LaCo_{12}B_6$ and $LaFe_{12}B_6$, studies on $GdCo_{12-x}Fe_xB_6$ compounds revealed the formation of the 1:12:6 phase up to $x = 3$ as well as an extreme sensitivity of the magnetic moment to the Fe doping [18]. For heavy rare earths like Ho, the maximum Fe content is further reduced to $x = 2$ [19].

All the interatomic distances discussed afterwards were obtained from the results of the Rietveld analysis of the X-ray diffraction patterns. The interatomic distances between the Y atoms and the Fe/Co atoms did not change upon increasing Fe concentration. However, we noticed that the distance between the Y(3*a*) and the Fe/Co(18*g*) was noticeably bigger than that with the Fe/Co of the 18*h* site (0.17 Å of difference). The distances between Fe/Co of the same 18*g* site proved to be the shortest in this series of compounds but were stable all along the Fe for Co substitution. This may indicate that Co is more present in this site. The case of the interatomic distances of Fe/Co atoms of the 18*h* site is as follows: 2 distances of multiplicity 2 are increasing while 1 distance of multiplicity 1 is decreasing. The general trend indicates a mean interatomic distance getting larger as the Fe concentration increases, meaning that Fe seems to occupy preferentially this crystallographic site. As for the Fe/Co interatomic distances between the 18*h* and 18*g* site, one distance increases then saturates around $x = 2.5$ where it

reaches a value > $2r_{Fe}$. The other 18*h*-18*g* distance seems to be decreasing really slowly with the Fe concentration. The X-ray measurement analysis did not allow us to refine the occupancy of Fe or Co in the two 18*g* and 18*h* sites. They were fixed according to the occupancies obtained by Mossbauer spectroscopy studies on $LaCo_{12-x}Fe_xB_6$ [3].

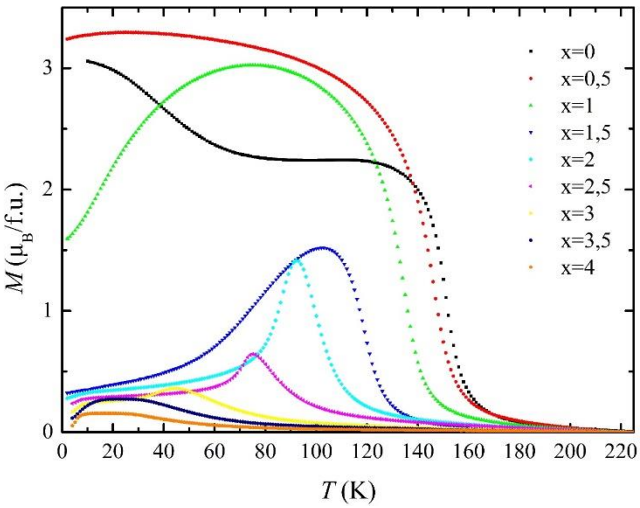

Figure 9: Thermomagnetic curves recorded under applied field of μ_0H = 0.1T along the $YCo_{12-x}Fe_xB_6$ series of compounds from x= 0 to 4.

Figure 9 presents a plot of the isofield magnetization curves recorded for all the studied $YCo_{12-x}Fe_xB_6$ compounds. The compound with x = 0 exhibits a magnetic transition at about 155 K a value in excellent agreement with that reported earlier by Rosenberg *et al.* [20]. According to these authors, $YCo_{12}B_6$ is a ferromagnet. It is worth to recall that $RCo_{12}B_6$ compounds are ferro- (R =Y, La-Sm) or ferri- (R = Gd-Tm) magnets and exhibit remarkably low ordering temperature for such high transition metal content (T_C =134 - 162 K) [6]. As can be seen from Figure 9 and Table 2, the Fe for Co substitution induces a significant reduction of the ordering temperature down to about 68 K for $YCo_{8.5}Fe_{3.5}B_6$ corresponding to a large decrease by almost a factor 3. For larger Fe concentration such as x = 4 the thermomagnetic curves plotted in Figure 9 indicates that the ordering temperature is further reduced. However its value is difficult to determine precisely due to the pronounced reduction of the magnetization and the smear out of the magnetic transition. Such decrease of T_C upon increasing Fe content in $YCo_{12-x}Fe_xB_6$ compounds recalls the behaviour observed for the $R_2Co_{14-x}Fe_xB$ compounds [21] another transition metal rich family of borides. On the contrary the influence of Fe for Co substitution in $YCo_{12-x}Fe_xB_6$ compounds behave differently from other R-Co-B compounds such as $YCo_{4-x}Fe_xB$ series for which an increase of both the ordering temperature and the saturation magnetization is observed upon increasing Fe concentration [22].

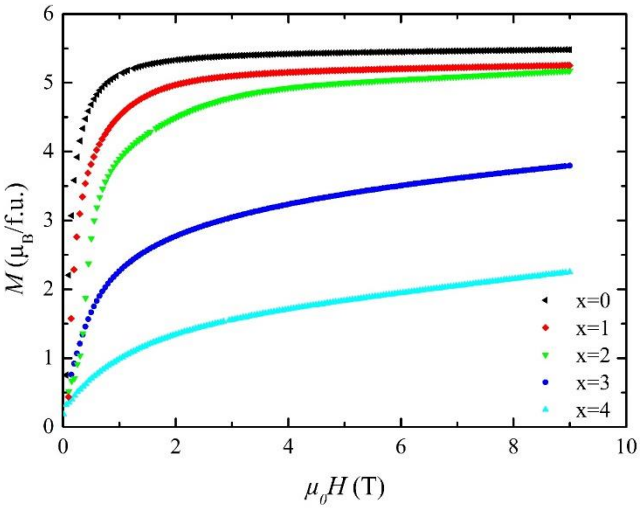

Figure 10: Magnetization curves measured at T = 4 K for the indicated compositions along the $YCo_{12-x}Fe_xB_6$ series of compounds

The isothermal magnetization curves recorded at 4 K for $YCo_{12-x}Fe_xB_6$ intermetallics are illustrated in Figure 10. The spontaneous magnetization was determined as the ordinate of the crossing point of the linearly extrapolated low- and high-field portions of the magnetization isotherms, i.e., by linear extrapolation to zero internal field. For $YCo_{12}B_6$ a spontaneous magnetization of 5.39 μ_B per formula unit is obtained; leading to an average magnetic moment of 0.45 μ_B per cobalt atom. This value is particularly reduced when compared to 1.8 μ_B/Co of elemental cobalt and even smaller than that reported for other R-Co-B borides. Indeed, a mean magnetic moment of 1.4 μ_B/Co and 0.69 μ_B/Co was obtained for $Y_2Co_{14}B$ [21, 23] and YCo_4B, respectively [22, 24, 25]. Figure 10 shows a progressive reduction of the magnetization upon increasing Fe content. The spontaneous magnetization at 4 K decreases from 5.39 to 0.89 μ_B/f.u. as x increases from 0 to 4. This clearly demonstrates the sensitivity of the magnetic properties to the substitution. It is worth recalling that in the $LaCo_{12-x}Fe_xB_6$ system, the magnetic order changes from ferromagnetic to antiferromagnetic for the Co and Fe rich side respectively [4,7,9].

The magnetization curves of Figure 10 for $YCo_{12-x}Fe_xB_6$ series of compounds have been obtained after correction of the ferromagnetic impurity signal. The estimation of the quantity of impurity traces has been done from Rietveld analysis of the X-ray diffraction pattern and isothermal magnetization curves recorded above T_C of the $YCo_{12-x}Fe_xB_6$ main phase. Indeed the impurity phase having a much higher ordering temperature (T_C = 426K [26] for $(Co,Fe)_2B$), its magnetic signal can be derived from such magnetic measurement and easily subtracted. Consequently the magnetization curves reported in this study have to be looked as reflecting the intrinsic magnetic properties of the $YCo_{12-x}Fe_xB_6$ phases. On Figure 10, the curvature of

the magnetization versus applied field measurements recorded for $x = 3$ and 4 are reflecting the reduction of the magnetization as well as the proximity to the ordering temperature whose value has been much reduced upon Fe for Co substitution. As can be seen from Figure 10, none of the $YCo_{12-x}Fe_xB_6$ compounds studied here are exhibiting large itinerant electron metamagnetic transition such as the one reported recently for $LaFe_{12}B_6$. The compounds richer than $x = 4$ have not been characterized in details from magnetic measurements since the presence of relatively large amount of impurities $(Co,Fe)_2B$ or α-Fe hampers to determine the intrinsic magnetic properties of the $R(Co,Fe)_{12}B_6$ phase of interest. More complete study of the intrinsic magnetic properties on single crystals would be interesting in order to get a deeper insight into the physical properties of $YCo_{12-x}Fe_xB_6$ series of compounds.

4. Conclusions

A series of $YCo_{12-x}Fe_xB_6$ alloy samples have been synthesized up to $x = 8$ and their crystal structure and chemical composition investigated combining different experimental techniques. Whereas a complete solid solution of iron has been reported for $LaCo_{12-x}Fe_xB_6$ isotype compounds our present study demonstrates that the Fe solubility limit is much lower in $YCo_{12-x}Fe_xB_6$ system and is estimated to about 4.5 Fe atom per formula unit. This solubility limit is found to be superior to that previously reported for R = Gd while the metallic radius of Y and Gd are almost identical (r_{Gd}=1.801 Å close to that of yttrium r_Y=1.773 Å [17]). All the lattice parameters are increased upon Fe for Co substitution a larger expansion being observed in the basal plane. The unit cell expands regularly at a rate of $\Delta V/V = 1.07$ % along the $YCo_{12-x}Fe_xB_6$ series of compounds. The precise substitution scheme of the Fe atom within the crystal lattice remains to be determined however the regular and even linear expansion of the unit cell as well as the solubility limit value below one half of the transition metal positions can be taken as a clue of a preferential occupation on one of the two inequivalent atomic positions. This has to be confirmed by other techniques such as neutron diffraction experiments for instance. All the $YCo_{12-x}Fe_xB_6$ compounds synthesized ($x < 4.5$) and studied here are exhibiting an overall net magnetization at low temperature and a ferromagnetic like behaviour. The Fe for Co substitution along the $YCo_{12-x}Fe_xB_6$ series of compounds induces a pronounced evolution of the magnetic properties with a dramatic reduction of the ordering temperature from 155 K down to less than 54 K for $x = 0$ and 4 respectively. In addition, the transition metal magnetization is also observed to diminish upon increasing the Fe concentration along the $YCo_{12-x}Fe_xB_6$ series of compounds.

Further magnetic studies such as neutron diffraction or Mössbauer spectroscopy may be interesting to investigate these compounds at the local scale and determine their precise magnetic structures. Study of local atomic environment also plays in favour of the existence of a preferential substitution scheme.

References

[1] K. Niihara and S. Yajima, Chem. Lett., **1**, 875 (1972).
[2] Y. B. Kuz'ma, G. V. Chernyak, and N. F. Chaban, Dopov. Akad. Nauk. Ukr., RSR **12**, 80-83 (1981).
[3] N.F. Chaban, K.Y. Val'chuk, and Y.B. Kuz'ma, Inorg. Mater., **31**, 848-850 (1995).
[4] M. Rosenberg, T. Sinnernann, M. Mittag, and K.H.J. Buschow, J. Alloys Compd., **182**, 145-156 (1992).
[5] K. H. J. Buschow, D. B. de Mooij, and H. M. van Noort, J. Less-Common Met., **125**, 135 (1986).
[6] M. Mittag, M. Rosenberg, K.H.J. Buschow, J. Magn. Magn. Mater., **82,** 109 (1989).
[7] L.V.B. Diop, O. Isnard, and J. Rodrıguez-Carvajal, Phys. Rev. B, **93**, 014440 (2016).
[8] L. V. B. Diop and O. Isnard, J. Appl. Phys., **119**, 213904 (2016).
[9] F. Mesquita, S.G. Magalhaes, P. Pureur, L.V.B. Diop, O. Isnard, Phys. Rev. B, **101**, 224414 (2020).
[10] L. V. B. Diop and O. Isnard, Appl. Phys. Lett., **108**, 132401 (2016).
[11] S. Fujieda, K. Fukamichi, and S. Suzuki, J. Magn. Magn. Mater., **421**, 403-408 (2017).
[12] J.M. Cadogan, S.J. Campbell, X.L. Zhao, and E. Wu, Aust. J. Phys., **46**, 679-88 (1993).
[13] L.V.B. Diop, Z. Arnold, O. Isnard, and J. Kamarád, J. Alloys Compd., **593**, 163-168 (2014).
[14] Z. Arnold, O. Isnard, H. Mayot, M. Misek, and J. Kamarad, J. Magn. Magn. Mater., **322**, 1117-1119 (2010).
[15] J. Rodriguez-Carvajal, Phys B: Condes. Matter, **192**, 55-69 (1993).
[16] Y. B. Kuz'ma and N.S. Bilonishko, Kristallografiya **16**, 1030 (1971).
[17] E. T. Teatum, K. A. Gschneidner Jr. and J. T. Waber, *COMPILATION OF CALCULATED DATA USEFUL IN PREDICTING METALLURGICAL BEHAVIOR OF THE ELEMENTS IN BINARY ALLOY SYSTEMS.*. United States: N. p. (1968).
[18] L. V. B. Diop, O. Isnard, N. R. Lee-Hone, D. H. Ryan and J. M. Cadogan, J. Phys.: Condens. Matter, **25**, 316001 (2013).
[19] L.V.B. Diop and O. Isnard, J. Alloys Compd., **804**, 392-395 (2019).
[20] M. Rosenberg, M. Mittag and K. H. J. Buschow, J. Appl. Phys., **63**, 3586-3588 (1988).
[21] J.F. Herbst, Rev. Modern Phys. **63**, 819 (1991)
[22] C. Chacon and O. Isnard, J. Appl. Phys., **89**, 71 (2001).
[23] D. Le Roux, H. Vincent, P. L'Heritier and R. Fruchart, J. Phys., Colloq., **46 (C6)**, C6-243-C6-247 (1985).
[24] H. Mayot, O. Isnard, Z. Arnold and J. Kamarad, J. Phys.: Condens. Matter. **20** 135207 (2008).

[25] A.T. Pedziwiatr, S.Y. Jiang, W.E. Wallace, E. Burzo and V. Pop, J. Magn. Magn. Mater., **66**, 69-73 (1987).

[26] A. Edström, M. Werwiński, D. Iuşan, J. Rusz, O. Eriksson, K. P. Skokov, I. A. Radulov, S. Ener, M. D. Kuz'min, J. Hong, M. Fries, D. Yu. Karpenkov, O. Gutfleisch, P. Toson, and J. Fidler, Phys. Rev. B, **92**, 174413 (2015); Erratum Phys. Rev. B **93**, 139901 (2016).